Miniaturized Wide- and Dual-Band Multilayer Electromagnetic Bandgap For Antenna Isolation and on-Package/PCB Noise Suppression

Petros Bantavis, Marc Le Roy, André Pérennec, Raafat Lababidi, Denis Le Jeune

▶ **To cite this version:**

Petros Bantavis, Marc Le Roy, André Pérennec, Raafat Lababidi, Denis Le Jeune. Miniaturized Wide- and Dual-Band Multilayer Electromagnetic Bandgap For Antenna Isolation and on-Package/PCB Noise Suppression. 2018 IEEE 22nd Workshop on Signal and Power Integrity (SPI)., May 2018, Brest, France. pp.1-4, 10.1109/SaPIW.2018.8401663 . hal-01821763

HAL Id: hal-01821763
https://hal.univ-brest.fr/hal-01821763

Submitted on 20 Sep 2018

HAL is a multi-disciplinary open access archive for the deposit and dissemination of scientific research documents, whether they are published or not. The documents may come from teaching and research institutions in France or abroad, or from public or private research centers.

L'archive ouverte pluridisciplinaire **HAL**, est destinée au dépôt et à la diffusion de documents scientifiques de niveau recherche, publiés ou non, émanant des établissements d'enseignement et de recherche français ou étrangers, des laboratoires publics ou privés.

Miniaturized Wide- and Dual-Band Multilayer Electromagnetic Bandgap For Antenna Isolation and on-Package/PCB Noise Suppression

Petros Bantavis, Marc Le Roy, *Member*, *IEEE*, André Perennec, Raafat Lababidi, *Member*, *IEEE*, Denis Le jeune
Lab-STICC UMR CNRS 6285,
Université de Brest (UBO)-ENSTA-Bretagne, Brest, France
Marc.LeRoy@univ-brest.fr

***Abstract*— This work presents a new design approach of wideband multilayer Electromagnetic Band Gaps (EBGs) suitable for both on package antenna isolation and switching noise suppression in high speed digital circuits. Depending on the target applications, the design principle is implemented from two conventional types of EBGs in order to improve their initial performance. By stacking multiple dielectric layers with integrated vias in both types of EBGs, it's possible to achieve dual band performance, to enhance the relative bandwidth of the first band gap and to miniaturize the unit cell. The dispersion diagrams of the multilayer EBGs are proposed and full-wave simulations are performed to validate the antenna isolation and noise suppression bandwidths of the final structures.**

Keywords*— *Antenna isolation; wide bandwidth; multi-layer stack; EBG; artificial-impedance surface; signal integrity; simultaneous switching noise; System-on-Package

I. Introduction

Electronics markets witness a continuous increasing need for highly integrated advanced devices which emphasizes the density of integration of different functional blocks in System-in-Package (SiP) or System-on-Package (SoP). Multiple technologies are combined in a same package, so that antennas and RF circuits have to coexist with analog and digital circuits with multiple interconnections and power distribution networks. Moreover, the associated signal integrity issues become more critical with increasing clock speeds and decreasing supply voltages. Several spurious couplings or noises may then occur both on the chip and in the package or PCB substrates. A generic technique is investigated here to overcome two of these issues.

First, at the antenna level in the RF front end, surface-wave leakage is one of the main sources of unwanted coupling between antennas. Electromagnetic Band Gaps (EBGs) are one of the best candidates to reduce this mutual coupling by eliminating the surface waves that are excited in the common dielectric substrate of the two antennas. Traditionally, such EBGs are suitable to isolate RX and TX antennas [1] but also to get high isolation between MIMO antennas [2] or to highly isolate RX and TX antennas in Full-Duplex (FD) systems [3]. Nevertheless, achieving a wideband isolation is still challenging.

On the other hand, SiP and SoP advanced technologies also require the suppression of noise coupling due to Simultaneous Switching Noise (SSN, also named power/ground noise). EBG structures that act as bandstop filters are also able to strongly reduce the noise likely to propagate in the Parallel-Plate Waveguide (PPW) formed by the power/ground planes. Thus, the design of compact wideband SSN canceller in power distribution network [4] is currently a major concern in mixed signal circuit design.

In this work, multilayer stacked EBGs are studied and it will be demonstrated that by increasing the number of dielectric layers, the unit-cell size becomes drastically smaller with respect to the bandgap wavelength. Moreover, the relative bandwidth of the bandgap increases and a second bandgap is produced at higher frequencies. Depending on the target applications, *i.e.* antenna isolation or SSN suppression, two types of EBGs will be implemented. An equivalent lumped model is proposed and extended to both configurations and validated by comparing the theoretical results to electromagnetic simulations and dispersion diagrams.

II. Generalized Multilayer EBG Design and Modelling

A. Multilayer model for wideband microwave applications

In planar antennas (*e.g.* microtrip antennas), surface wave modes are excited in the dielectric substrate at the antenna edges. Several topologies of EBGs with vias have been investigated to suppress the TM and TE surface-wave modes that are able to propagate in such a grounded dielectric slab. Here, a square lattice was selected due to its wider bandwidth [5]. In single-dielectric-layer mushroom EBG as illustrated in Fig. 1a, the unit cell (Fig.1.b) and the surface impedance are usually modelled by an LC resonant circuit to express the centre angular frequency ω_0, the bandwidth BW, and the impedance surface Z. The inductance value L_T is related to the substrate thickness and permeability while the gap capacitance C is related to the mushroom and gap dimensions and substrate permittivity. Approximate closed-form equations and the design procedure are given in [5]. Several approaches, such as mushroom with overlapping plates [6] or unidimensional [7] were proposed to reduce the dimension of the cell by increasing the capacitance value but at the expense of the relative bandwidth. Indeed, reducing the cell size while simultaneously widening the bandwidth requires higher capacitance and inductance per unit cell values.

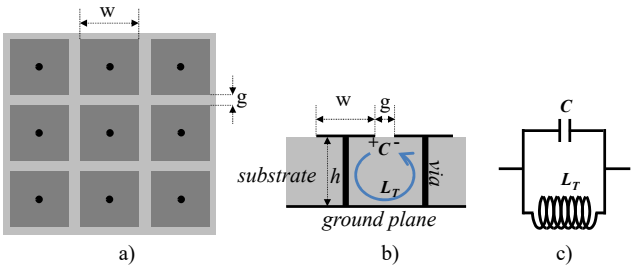

Fig. 1. (a) Top-view of a classical single layer EBG. (b) Side-view and behaviour of a unit cell. (c) Equivalent lumped model of a unit-cell.

$$\omega_0 = \frac{1}{\sqrt{L_T C}} \tag{1}$$

$$BW = \frac{\Delta\omega}{\omega_0} = \frac{\sqrt{L_T / C}}{\sqrt{\mu_0 \varepsilon_0}} \tag{2}$$

$$Z = j\frac{\omega L_T}{1-\omega^2 L_T C} \tag{3}$$

Here, a multilayer EBG (M-EBG) structure is proposed in two configurations (Fig. 2a and 2b). This structure allows increasing simultaneously the inductance and capacitance values to reduce the cell size while keeping a wide surface-wave stop-band bandwidth suitable for both intended applications.

As a first approximation, the capacitances C between adjacent mushrooms are considered equal regardless of the layer position (top and intermediate layers). The inductance L_T (defined from the single layer configuration) is subdivided into three parts (Fig. 2.a) that correspond to the vias and ground contributions, L_V and L_G, respectively; *i.e.* $L_T = L_G + 2L_V$. Thus, a multilayer lumped equivalent model of the surface impedance can be expressed as detailed in Fig. 2.a. Starting from the single layer admittance $Y_1 = jB_1$ with the initial conditions $B_G = -1/(\omega L_G)$, the 2-layer admittance Y_2 can be deduced as a function of B_1 and so on and so forth, as explained in Fig. 2a. For an n layer-stack, the surface impedance Z_n or admittance $Y_n = jB_n$ is purely reactive which is expressed by (4). As in the case of a single layer EBG, this multilayer lumped representation only estimates the central frequency of the first bandgap as well as the impedance surface.

$$B_n = C\omega + \cfrac{1}{-2L_V\omega + \cfrac{1}{C\omega + \cfrac{1}{-2L_V\omega + \cfrac{1}{\ddots + \cfrac{1}{-(2L_V + L_G)\omega}}}}} \quad \left.\right\} n \text{ iterations} \tag{4}$$

This stack-model can be applied to design a wideband surface-wave isolation between wideband planar circuits, typically microstrip antenna array, *i.e.* where the top guiding structure is initially a grounded dielectric slab.

B. Multilayer EBG model for wideband SSN suppression

Simultaneous Switching Noise (SSN) occurs between two reference planes due to high speed voltage and current switching in digital sections of PCB and packages (SiP/SoP). In this case, high speed switching excites modes in a Parallel-Plate Waveguide (PPW) formed by the power distribution network. The structure understudy (Fig. 2b) consists of a PPW where the bottom metallic plate is replaced by the n-layer stacked EBG studied in the previous section. Our objective here is to estimate the bandgap and its central frequency by extending the model of EBG-grounded dielectric slab studied in the previous section to this PPW configuration by using the transverse resonance method (TRM) [8]-[9]. TRM was initially developed to study waveguides with inhomogeneous transverse-section waveguide. The multilayer structure (PM-EBG) is investigated by using the TRM to model the continuity of electric and magnetic fields in the transverse directions by an equivalent resonant circuit with transmission lines. As shown in Fig. 2c, a cross section of the whole structure can be modelled by the surface impedance $Z_{-x} = Z_n = -j/B_n$ when looking into the n-layer EBG direction (x<0); and by a transmission line with a characteristic impedance Z_w when (x>0).

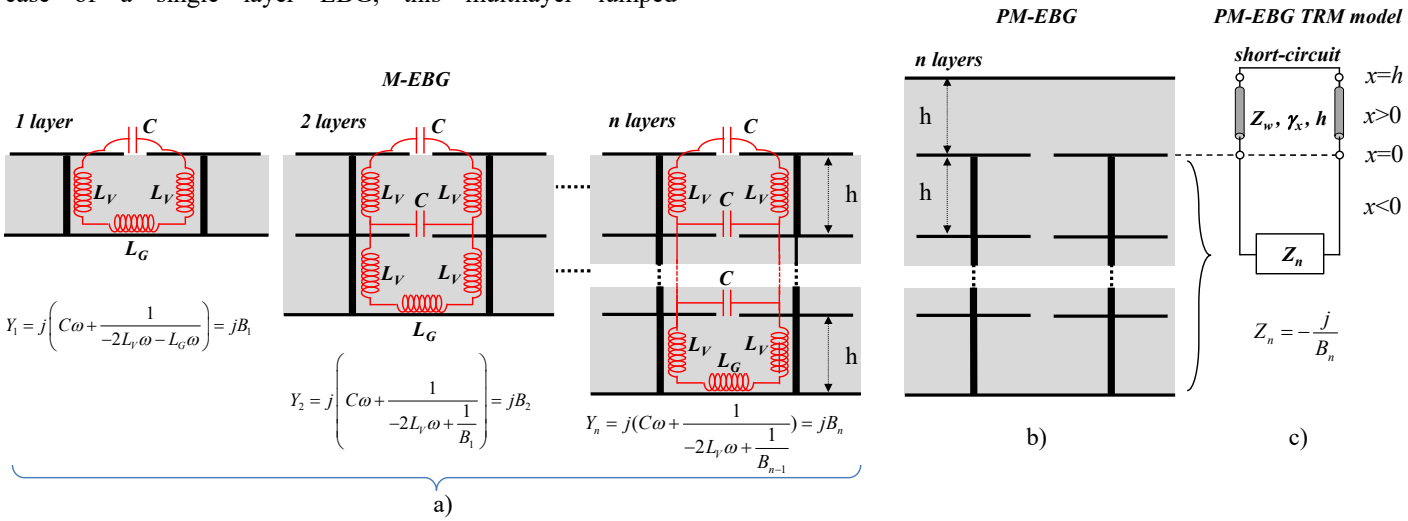

Fig. 2. (a) Multilayer EBG (M-EBG) and the corresponding lumped-modelling. (b) Power-plane Multilayer EBG (PM-EBG) side view, with its equivalent TRM transmission line model (c).

Z_w corresponds to the wave impedance of the type of modes, *i.e.* TEM, TM_n and TE_n in a PPW. The transmission line is loaded by a short circuit which represents the metal plate at $x=h$. Such a short-circuited stub of length h along x presents input impedances Z_{+x} associated to the transverse wave number γ_x:

$$Z_{+x}^{TM} = -j\frac{\gamma_x}{\omega\varepsilon}\tanh(\gamma_x h) \tag{5a}$$

$$Z_{+x}^{TE} = j\frac{\omega\mu_0}{\gamma_x}\tanh(\gamma_x h) \tag{5b}$$

Where $\gamma_x^2 = \beta^2 - k^2$, with $k^2 = \omega^2\mu_0\varepsilon_0\varepsilon_r$, and γ_x is purely imaginary for TE modes in (5b) and real in (5a) for TM modes. The first mode is a TEM mode which starts from DC and then becomes TM_0 up to the bandgap which corresponds to (5a), whereas (5b) is for the second mode, *i.e.* TE_1 that propagates after the resonance. The resonance condition of the TRM requires that the impedance seen when looking in one transverse direction (*e.g.* $x<0$) at the interface is the opposite of the impedance seen in the other direction ($x>0$):

$$Z_{-x} + Z_x = 0 \tag{6}$$

Inserting (4), (5a) or (5b), into (6) provides after simplification the dispersion relations for the power-plane EBG waveguide:

For TM_0:
$$-\frac{1}{B_n} - \frac{\sqrt{\beta^2 - \omega^2\mu_0\varepsilon_0\varepsilon_r}}{\omega\varepsilon_0\varepsilon_r}\tanh\left(\sqrt{\beta^2 - \omega^2\mu_0\varepsilon_0\varepsilon_r}\,.h\right) = 0 \tag{7a}$$

For TE_1:
$$-\frac{1}{B_n} + \frac{\omega\mu_0}{\sqrt{\omega^2\mu_0\varepsilon_0\varepsilon_r - \beta^2}}\tan\left(\sqrt{\omega^2\mu_0\varepsilon_0\varepsilon_r - \beta^2}\,.h\right) = 0 \tag{7b}$$

Dispersion diagrams can be obtained by solving these transcendental equations for a different number of layers. The cutoff frequencies of the TE_1 modes can be directly obtained by solving (7b) for $\beta = 0$. In the next section, a validation of both the surface impedance lumped-model for the M-EBG structure and of the TRM modelling for the PM-EBG one is carried out by comparison to corresponding dispersion diagrams from a commercial eigenmode solver and full-wave electromagnetic (EM) simulations of a practical case.

III. Validation of Multilayer-Lumped and TRM Models by Comparison to EM Simulations

A. M-EBG lumped-model simulation results and validation

Fig. 3 shows the dispersion diagram (the triangle ΓXM, corresponds to the irreducible Brillouin zone) calculated by using the eigenmode solver of CST Studio for the unit cell made up of 1 and 3 layers of Fig. 2a.

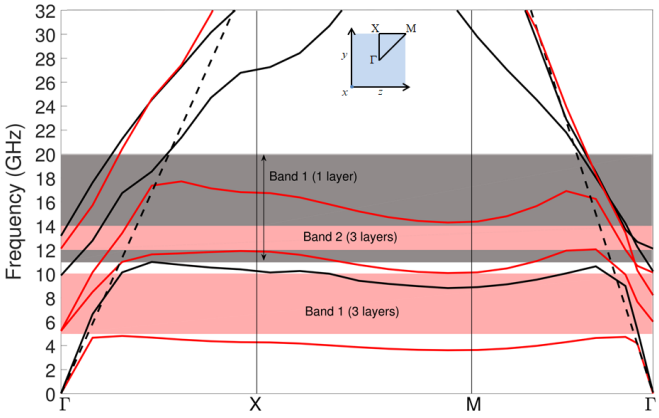

Fig. 3. M-EBG dispersion diagrams for 1 and 3 layers. Cell size: w=2.25 mm, g =0.3 mm, ϕ_{via} = 200 µm, h=1.6 mm, metal thickness t=35 µm, ε_r=2.2.

The single layer EBG produces a unique bandgap from 11 to 20 GHz with a relative bandwidth of 58%. For three layers, a dual-band performance is achieved where the first band gap ranges from 5 to 10 GHz with a relative bandwidth of 66.6%. Thus, this behavior corresponds to a minimization of the unit cell size since the band gap appears at a lower frequency band, with an enhanced relative bandwidth. Additionally, a second band gap is produced in the 12-14 GHz band. The results obtained by following the same procedure for 3 up to 10 layers are summarized for clarity in Table I. Indeed, adding multiple stacked layers confirms that the resonance frequency for both band gaps is decreased and the relative bandwidth for the first one is slightly increased. Full ElectroMagnetic (EM) simulations were also carried out in a practical case (a finite 5x5 EBG structure from 1 to 10 layers with a coplanar line excitation) and the results fit accurately the dispersion diagrams while showing a high isolation level in the band gap. Table I sums up the bandgap frequencies and bandwidths versus the number of stacked layers. In order to verify the proposed lumped model, L_T, L_V, L_G, and C are first estimated from classical closed-form equations [5], [10]-[11]. For the structure and cell dimensions specified in Fig. 3, the following component values are extracted: L_T= 2.01 nH, L_V= 658 pH, L_G= 693 pH, C = 56.1 fF. Then, the resonance frequencies of the equivalent lumped model (dot curves in Fig. 5) are extracted from (4) and found to be consistent with the bandgap central-frequencies from eigenmode solver/EM simulations.

B. PM- EBG TRM model and dispersion diagrams

The same approach to calculate using CST the resonant frequencies of eigenmodes along the Brillouin zone is applied to the PM-EBG structure (Fig. 2b) with identical dimensions and substrate layers to get the dispersion diagrams from 1 to 10 layers.

TABLE I: Bandwidths (*BW*) and bandgaps obtained from dispersion diagrams for one to ten layers for M-EBG and PM-EBG.

	Number of layers	1	2	3	4	5	6	7	8	9	10
M-EBG	1st Bandgap (GHz)	11-20	6.7-13.2	5-10	3.6-8	3.3-6.5	2.5-6.4	2.4-4.9	2.1-4.5	2-4.5	1.8-3.8
	2nd Bandgap (GHz)	-	-	12-14	10-12.2	9-10.5	8.1-9.5	7.5-9.6	7.1-8.2	6.5-7.2	5-5.7
	BW (%)	58	65.3	66.6	75.8	65	67.4	68.4	72.7	76.9	71.4
PM-EBG	1st Bandgap (GHz)	8-23	5.9-17.4	4.7-14	3.9-12.2	3.4-10	3-9.2	2.6-8.2	2.4-7.3	1.9-5.9	1.8-5.6
	2nd Bandgap (GHz)	-	-	17.2-19	15.1-17.5	13-16	11.4-14.4	10-13	9-11.2	8.2-9.5	6.5-8.1
	BW (%)	96.7	98.7	99.4	103.1	98.5	101.6	103.7	101	102.5	102.7

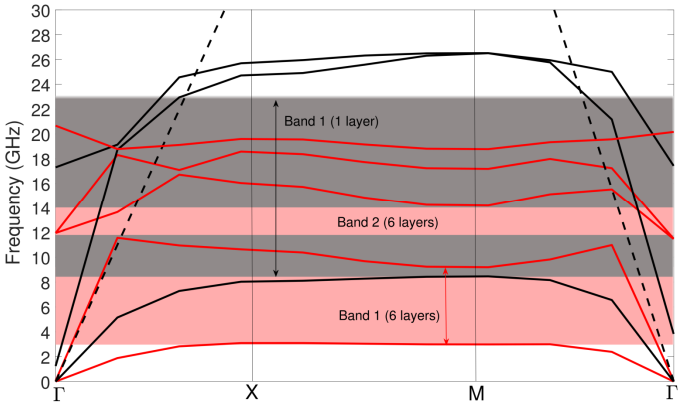

Fig. 4. PM-EBG Dispersion diagrams for 1 and 6 layers.

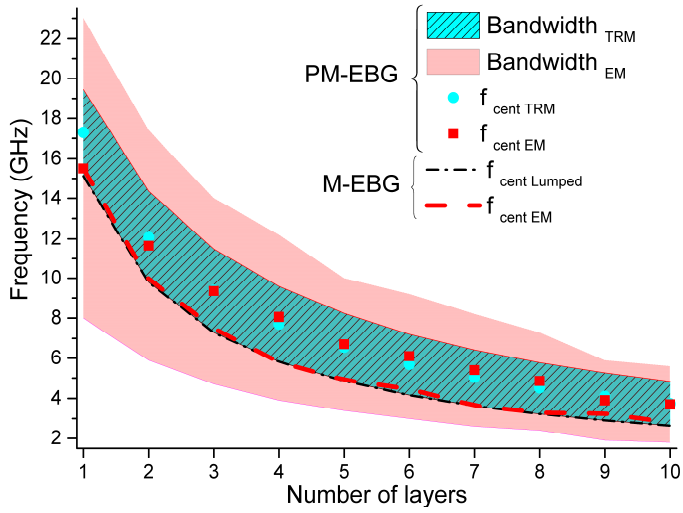

Fig. 5. Comparison of central frequencies and bandwidths for M-EBG and PM-EBG from equivalent models and dispersion diagrams.

Identical global trends as in section III-A are evidenced in Fig. 4 (only dispersion diagrams for n = 1 and 6 layers are plotted for clarity) and in table I, *i.e.* a wide relative bandwidth that slightly increases versus *n* with a strong shift to lower frequencies of these stopbands. A 2nd bandgap is also created and follows identical behaviors. By using (7a) and (7b) with the aforementioned lumped components values, the dispersion bandgaps are calculated following the TRM principle. Fig. 5 illustrates the obtained results in comparison with eigenmode solver ones (hatched areas for the bandwidth and scatters for the central frequencies). The bandgap lower edge is estimated from TRM with (7a) for TM_0 mode which is actually the lower resonance frequency of Z_n; whereas the cutoff frequency of TE_1 defines the bandgap upper bound. The TRM center frequencies are consistent with those from CST whereas the relative bandwidths follow the same global trend with a slight increase. But nevertheless, the bandwidths from TRM method are under evaluated as in [8]. A part of the discrepancies in bandgap bound estimation comes from the approximate values of the lumped components. Moreover, the EBG in TRM is considered as an equivalent uniform surface defined by Z_n which implies that this approximation provides better results when the wavelength is big compared to the cell size, which is confirmed for $n = 10$ in Fig. 5.

IV. Conclusion

In this paper, a generalized design of multilayer stacked EBGs for wideband applications is presented and then dedicated respectively to mitigate the coupling between on package/PCB RF circuits such as Tx/Rx antennas and also to reduce the SSN between power planes in high-speed digital systems in SiP/SoP technologies. Both multilayer implementations proved that increasing the number of stacked dielectric layers with integrated vias results in a dual band performance, minimizes the unit cell size and enhances the relative bandwidth of the first band gap. Moreover, an equivalent lumped model of the multi-layer EBG structure is proposed in this paper and extended by TRM to the power-plane configuration. Furthermore, the two models are validated by a comparison to dispersion diagrams. This approach can be applied to any EBG to gain in compactness and bandwidths. This allows the implementation of miniaturized, high-level and wideband isolation structure between planar MIMO antennas or in Full-Duplex transceivers, as well as wideband SSN canceller in multi-layers and -packages digital/mixed systems. Such multilayer EBGs have then the ability to limit the surface wave propagation over a wide bandwidth in order to reduce the unwanted coupling between antennas or to provide artificial impedance surfaces to improve antenna design [5].

References

[1] Fan Yang and Y. Rahmat-Samii, "Microstrip antennas integrated with electromagnetic band-gap (EBG) structures: A low mutual coupling design for array applications ," *IEEE Trans. Antennas Propag.*, vol. 51, no 10, pp. 2936-2946, oct. 2003.

[2] M.-H. Hsu, T.-C. Tang, and K.-H. Lin, "EBG reflector-backed MIMO antenna with wideband isolation and uni-directional radiation pattern MIMO antenna for MIMO radar ," *IEEE Antennas and Propagation Society International Symposium*, pp. 612–613, 2013.

[3] B. Debaillie, D.J. van den Broek, C. Lavín, B. van Liempd, E.A.M. Klumperink, C. Palacios, J. Craninckx, and B. Nauta, "RF Self-Interference Reduction Techniques for Compact Full Duplex Radios ," *2015 IEEE 81st Vehicular Technology Conference*, pp. 1-6, 2015.

[4] M. Kim, K. Koo, C. Hwang, Y. Shim, J. Kim, and J. Kim, "A Compact and Wideband Electromagnetic Bandgap Structure Using a Defected Ground Structure for Power/Ground Noise Suppression in Multilayer Packages and PCBs ," *IEEE Trans. Electromagn. Compat.*, vol. 54, no 3, pp. 689-695, juin 2012.

[5] C. A. Balanis, Advanced engineering electromagnetics, 2nd ed. Hoboken, N.J: John Wiley & Sons, 2012.

[6] D. Sievenpiper, L. Zhang, R. F. Broas, N. G. Alexopolous, and E. Yablonovitch, "High-impedance electromagnetic surfaces with a forbidden frequency band ," *IEEE Trans. Microw. Theory Tech.*, vol. 47, no 11, pp. 2059–2074, 1999.

[7] B. Mohajer-Iravani and O. M. Ramahi, "Wideband Circuit Model for Planar EBG Structures ," *IEEE Trans. Adv. Packag.*, vol. 33, no 1, pp. 169-179, feb. 2010.

[8] R. Abhari and G. V. Eleftheriades, "Metallo-dielectric electromagnetic bandgap structures for suppression and isolation of the parallel-plate noise in high-speed circuits ," *IEEE Trans. Microw. Theory Tech.*, vol. 51, no 6, p. 1629-1639, juin 2003.

[9] R. Sorrentino, "Transverse Resonance Technique," in Numerical Techniques for Microwave and Millimeter- Wave Passive Structures, T. Itoh, Ed., New York: Wiley, 1989, ch. 11.

[10] B. Young, Digital Signal Integrity: Modeling and Simulation with Interconnects and Packages, Prentice Hall PTR, 2001.

[11] M. E. Goldfarb and R A. Pucel, "Modeling via hole grounds in microstrip," *IEEE microwave and guided wave letters*, vol. 1, no 6, pp. 135-137, 1991.